Computational Mechanics manuscript No.
(will be inserted by the editor)

New anisotropic crack-tip enrichment functions for the extended finite element method

G. Hattori · R. Rojas-Díaz · A. Sáez · N. Sukumar · F. García-Sánchez

Received: date / Accepted: date

Abstract In this paper, the extended finite element method (X-FEM) is implemented to analyze fracture mechanics problems in elastic materials that exhibit general anisotropy. In the X-FEM, crack modeling is addressed by adding discontinuous enrichment functions to the standard FE polynomial approximation within the framework of partition of unity. In particular, the crack interior is represented by the Heaviside function, whereas the crack-tip is modeled by the so-called crack-tip enrichment functions. These functions have previously been obtained in the literature for isotropic, orthotropic, piezoelectric and magnetoelectroelastic materials. In the present work, the crack-tip functions are determined by means of the Stroh's formalism for fully anisotropic materials, thus providing a new set of enrichment functions in a concise and compact form. The proposed formulation is validated by comparing the obtained results with other analytical and numerical solutions. Convergence rates for both topological and geometrical enrichments are presented. Performance of the newly derived enrichment functions is studied, and comparisons are made to the well-known classical crack-tip functions for isotropic materials.

G. Hattori · R. Rojas-Díaz · A. Sáez
Department of Continuum Mechanics, School of Engineering, University of Seville
Camino de los Descubrimientos s/n, 41092, Seville, Spain
E-mail: rrojasdiaz@us.es

N. Sukumar
Department of Civil and Environmental Department, One Shields Avenue, Davis, CA 95616. U.S.A.

F. García-Sánchez
Departamento de Ingeniería Civil, de Materiales y Fabricación, E.T.S. de Ingenieros Industriales, Universidad de Málaga, Doctor Ortiz Ramos, 29071-Málaga, Spain

Keywords Crack-tip enrichment functions · Anisotropic materials · X-FEM · Stroh's formalism

1 Introduction

The strong demand for materials with a high strength per unit weight ratio in different branches of engineering has led to the development of different analytical and numerical techniques to solve fracture mechanics problems in anisotropic materials. Pioneering works by Muskhelishvili [15] and Sih et al. [20], or more recently, works by Nobile and Carloni [16], developed analytical techniques to solve crack problems in anisotropic and orthotropic plates. However, these methods are limited to simple geometries and load combinations. Therefore, numerical methods become essential to analyze more complicated engineering applications. In particular, models based on the boundary element method (both the classical [22] and the dual [11,17,23] approximations), meshless (meshless local Petrov-Galerkin [21]), and the finite element method (FEM) [7], have been developed.

All the above-mentioned numerical techniques have proven to be accurate and robust to solve crack problems. However, in the case of the FEM, its direct application is unwieldly, since the mesh must conform to the crack geometry, mesh refinement is required near the crack-tip, and for crack propagation simulations, remeshing is needed. To circumvent these difficulties, the extended finite element method (X-FEM), first presented by Belytschko and co-workers [6,13], has emerged as a powerful alternative in computational fracture. It has been successfully applied to solve crack problems in materials with different constitutive laws: see, for ex-

ample, the works by Moës et al. [13] in isotropic media, Sukumar et al. [25] in bimaterials, Asadpoure and Mohammadi [2] in orthotropic materials, Béchet et al. [5] in piezoelectric solids and Rojas-Díaz et al. [19] in magnetoelectroelastic materials. Abbas and Fries [1] have obtained enrichment functions that can be applied to brittle as well as cohesive cracks. In the X-FEM, additional (enrichment) functions are added to the classical finite element polynomial approximation through the framework of partition of unity [3]. To model the crack discontinuity, the crack interior is represented by a discontinuous (Heaviside) function, whereas the behavior around the crack-tip is modeled by the asymptotic crack-tip enrichment functions.

In this work, a new set of crack-tip enrichment functions is derived to simulate two-dimensional elastic fracture in general anisotropic media. These new functions are obtained in a concise and compact form in terms of the Stroh's formalism [24]. The resulting formulation is validated by comparison of the obtained results for several crack configurations with previous analytical and/or numerical solutions. Two different enrichment strategies have been adopted: the conventional X-FEM using a topological enrichment and a geometrical (fixed area) enrichment [4,12]. Convergence rates for both enrichments are presented and performance of the newly derived enrichment functions is further analyzed and compared with the classical crack-tip functions for isotropic materials.

The paper is structured as follows. The governing equations are stated in Section 2. The theoretical foundations of the X-FEM are presented in Section 3, and the new crack-tip enrichment functions are derived in Section 4 and the computation of fracture parameters using the domain form of the contour interaction integral is briefly described in Section 5. Several crack problems are solved in Section 6 to validate the approach and characterize its convergence. The main conclusions from this study are summarized in Section 7.

2 Governing equations

2.1 Basic equations

In an anisotropic elastic domain, the static equilibrium equations in the presence of body forces $\mathbf{b}$ are given by

$$\sigma_{ij,j} + b_i = 0 \tag{1}$$

Both the stress and strain tensors are symmetric: $\sigma_{ij} = \sigma_{ji}$; $\varepsilon_{ij} = \varepsilon_{ji}$.

$$\varepsilon_{ij} = \frac{1}{2}(u_{i,j} + u_{j,i}) \tag{2}$$

The linear constitutive relations between stresses σ_{ij} and strains ε_{kl} are given by the generalized Hooke's law

$$\sigma_{ij} = C_{ijkl}\varepsilon_{kl} \tag{3}$$

where C_{ijkl} define the material constants tensor, satisfying the following symmetry relations

$$C_{ijkl} = C_{jikl} = C_{ijlk} = C_{klij} \tag{4}$$

that lead to a tensor with only 21 independent components for the 3D case, and 6 components in the 2D case.

2.2 Stroh's formalism

To satisfy the equilibrium equations stated in (1), the displacement field in a generally anisotropic plane domain may be written as [24, 27]

$$\mathbf{u} = \mathbf{a}f(z) \tag{5}$$

where $z = x_1 + \mu_m x_2$ is the transformation into the complex plane of the physical coordinates (x_1, x_2), and μ_m represents the complex roots with positive imaginary part, of the characteristic equation of the material. Such an equation follows from derivation of (5), and subsequent substitution of (3) into the equilibrium relations (1), leading to

$$\{\mathbf{Z} + (\mathbf{M} + \mathbf{M}^T)\mu_m + \mathbf{L}\mu_m^2\}\mathbf{a} = \mathbf{0} \tag{6}$$

with

$$\mathbf{Z} := \mathbf{C}_{1ij1}; \quad \mathbf{M} := \mathbf{C}_{2ij1}; \quad \mathbf{L} := \mathbf{C}_{2ij2} \tag{7}$$

Equation (6) can be rearranged and further expressed as the following eigenvalue problem

$$\left(\begin{array}{c|c} -\mathbf{L}^{-1}\mathbf{M} & -\mathbf{L}^{-1} \\ \hline \mathbf{Z} - \mathbf{M}^T\mathbf{L}^{-1}\mathbf{M} & -\mathbf{M}^T\mathbf{L}^{-1} \end{array}\right)\left(\frac{\mathbf{A}_m}{\mathbf{B}_m}\right) = \mu_m\left(\frac{\mathbf{A}_m}{\mathbf{B}_m}\right) \quad \text{(no sum on } m\text{)} \tag{8}$$

Since the tensors $\mathbf{A}$ and $\mathbf{B}$ and the eigenvalues μ_m depend only on the material properties, they are independent of the geometrical position of the adopted coordinated system. These characteristics allow the calculation of precise and general terms by means of the Stroh's formalism.

2.3 Asymptotic fields around the crack-tip

The asymptotic displacement field around a crack-tip in a plane anisotropic domain was first derived by Sih et al. [20]. Adopting a polar coordinate system (r, θ) with origin at the crack-tip, the displacement field can be expressed by means of the Stroh's formalism [26] as

$$u_i(r,\theta) = \sqrt{\frac{2}{\pi}} \Re \left(K_\alpha A_{im} B^{-1}_{m\alpha} \sqrt{r\left(\cos\theta + \mu_m \sin\theta\right)} \right) \tag{9}$$

where the summation convention over repeated indices holds; $i, m = 1, 2$; $\alpha = I, II$ is associated with the fracture modes; and $\Re(\cdot)$ is the real part of $(\cdot)$.

Similarly, the asymptotic stress fields may be written as

$$\sigma_{ij}(r,\theta) = (-1)^j \sqrt{\frac{1}{2\pi}} \Re \left(K_\alpha B_{im} B^{-1}_{m\alpha} \frac{\delta_{j1}\mu_m + \delta_{j2}}{\sqrt{r\left(\cos\theta + \mu_m \sin\theta\right)}} \right) \tag{10}$$

where δ_{jk} is the Kronecker-delta.

3 Extended finite element formulation

Equation (10) reveals that the discontinuity induced by the crack leads to a non-smooth behavior of the field variables, with resulting singular gradient that needs to be taken into account. For this purpose, the extended finite element method [6, 13] is adopted in which the classical FEM polynomial space is enriched through the framework of partition of unity [3] with the addition of special shape functions: the crack jump is represented by a discontinuous (Heaviside) function and the crack-tip $\sqrt{r}$-behavior is modeled by asymptotic crack-tip enrichment functions. In this way, the FE mesh does not need to match the crack geometry and only a subset of nodes close to the crack needs to be enriched. Currently, the X-FEM is a well-established technique and its advantages over conventional FEM for problems with non-smooth behavior are well-recognized [10].

3.1 Crack modeling and selection of enriched nodes

Consider a domain $\Omega \subset \mathbf{R}^2$ with boundary Γ, which contains a crack $\Gamma_c = \Gamma_c^- \cup \Gamma_c^+$. The domain is discretized by finite elements, so that $\mathcal{N}$ denotes the nodal set. Displacements are prescribed on Γ_u, whereas tractions are imposed on Γ_t, so that $\Gamma = \Gamma_u \cup \Gamma_t$ as illustrated in Figure 1. The displacement approximation in the X-FEM can be written as [13]

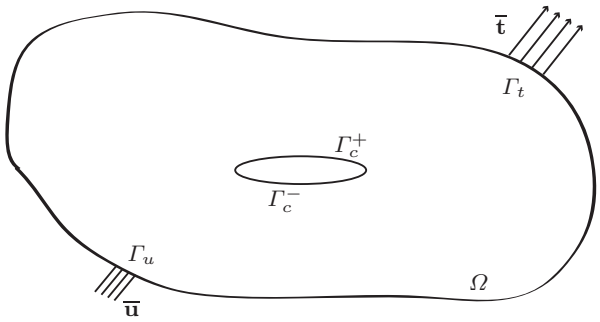

Fig. 1 Boundary-value problem with an internal crack.

$$\mathbf{u}^h(\mathbf{x}) = \sum_{i\in\mathcal{N}} N_i(\mathbf{x})\mathbf{u}_i + \sum_{j\in\mathcal{N}^{\mathcal{H}}} N_j(\mathbf{x})H(\mathbf{x})\mathbf{a}_j + \sum_{k\in\mathcal{N}^{\mathcal{CT}}} N_k(\mathbf{x}) \sum_{\alpha} F_\alpha(\mathbf{x})\mathbf{b}_k^\alpha \tag{11}$$

where N_i is the standard finite element shape function associated with node i, $\mathbf{u}_i$ is the vector of nodal degrees of freedom for classical finite elements, and $\mathbf{a}_j$ and $\mathbf{b}_k^\alpha$ are the added set of degrees of freedom that are associated with enriched basis functions. $H(\mathbf{x})$ is the generalized Heaviside function, defined as $+1$ or -1, depending on whether it is evaluated above or below the crack, respectively. The Heaviside function thus enables modeling of a crack that fully cuts a finite element. Additionally, at the nodes around the crack-tip, crack-tip functions $F_\alpha(\mathbf{x})$ are included. They are described in more detail in Section 4. In elastic materials, $\mathbf{b}_k^\alpha$ is an 8-component vector for two-dimensional problems, since only two nodal variables (u_1, u_2) and four enrichment functions are needed to describe all the possible deformation states in the vicinity of the crack-tip. This holds for both the well-known isotropic crack-tip functions [13] as well as for the orthotropic [2] and fully anisotropic cases, as will be shown next.

Figure 2 illustrates the classical topological enrichment strategy [13] to model a crack in the X-FEM. The nodes that are enriched with the Heaviside function (set $\mathcal{N}^H$) are marked with a filled circle and they belong to elements fully cut by the crack. The nodes that are enriched with crack-tip enrichment functions (set $\mathcal{N}^{CT}$) are marked with a square and they belong to elements that contain the crack-tip.

More recently, an alternative enrichment strategy that leads to improved results was proposed by Laborde et al. [12] (geometrical enrichment): some nodes around the ones belonging to the elements that contain the

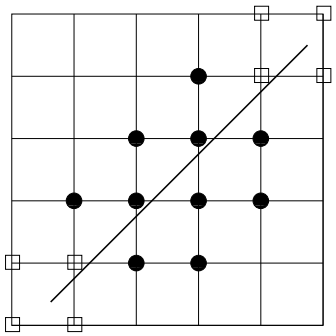

Fig. 2 Node selection for topological enrichment.

crack-tips are also enriched with the crack-tip functions, in order to improve the convergence of the method. Here we adopt a fixed area enrichment, so that all nodes lying inside a circle of diameter $2r_e$ centered at the crack-tip are enriched with the crack-tip functions, as is depicted in Figure 3.

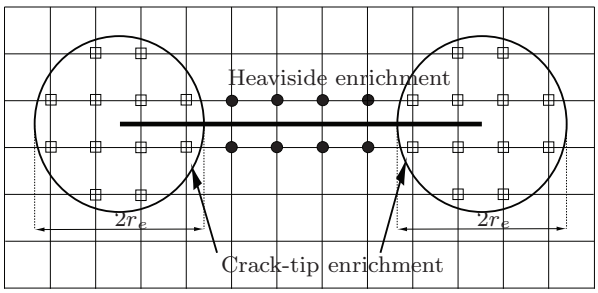

Fig. 3 Node selection for geometrical enrichment.

3.2 Weak formulation and discrete equations

Let $\mathbf{u}$ be the displacement vector and $\boldsymbol{\sigma}$ the stress tensor. The weak form (principle of virtual work) for a continuum elastostatic problem in a general anisotropic solid is given by

$$\int_{\Omega} \boldsymbol{\sigma} : \delta\boldsymbol{\varepsilon}\, d\Omega = \int_{\Gamma_t} \overline{\mathbf{t}} \cdot \delta\mathbf{u}\, d\Gamma + \int_{\Omega} \mathbf{b} \cdot \delta\mathbf{u}\, d\Omega \tag{12}$$

where δ is the variation operator, $\overline{\mathbf{t}}$ is the prescribed traction vector and $\mathbf{b}$ are the body forces. On substituting the trial and test approximations in the above equation, and using the arbitrariness of nodal variations, we obtain the discrete equations:

$$\mathbf{K}\mathbf{d} = \mathbf{f} \tag{13}$$

where $\mathbf{K}$ is the global stiffness matrix and $\mathbf{f}$ is the force vector.

The element contribution to $\mathbf{K}$ and $\mathbf{f}$ are as follows:

$$\mathbf{k}_{ij}^{e} = \begin{bmatrix} \mathbf{k}_{ij}^{uu} & \mathbf{k}_{ij}^{ua} & \mathbf{k}_{ij}^{ub} \\ \mathbf{k}_{ij}^{au} & \mathbf{k}_{ij}^{aa} & \mathbf{k}_{ij}^{ab} \\ \mathbf{k}_{ij}^{bu} & \mathbf{k}_{ij}^{ba} & \mathbf{k}_{ij}^{bb} \end{bmatrix} \tag{14a}$$

$$\mathbf{f}_{i}^{e} = \{\mathbf{f}_{i}^{u}\ \mathbf{f}_{i}^{a}\ \mathbf{f}_{i}^{b\alpha}\}^{T} \quad (\alpha = 1, 4) \tag{14b}$$

where the indices u, a, b refer to the nodal displacements vector, the Heaviside enriched nodes and the crack-tip enriched nodes, respectively.

$$\mathbf{k}_{ij}^{rs} = \int_{\Omega_e} (\mathbf{B}_i^r)^T \mathbf{C} (\mathbf{B}_i^s)\, d\Omega \quad (r, s = u, a, b) \tag{15a}$$

$$\mathbf{f}_{i}^{u} = \int_{\partial\Omega_e} N_i \overline{t} d\Gamma + \int_{\Omega_e} N_i \mathbf{b} d\Omega \tag{15b}$$

$$\mathbf{f}_{i}^{a} = \int_{\partial\Omega_e} N_i H \overline{t} d\Gamma + \int_{\Omega_e} N_i H \mathbf{b} d\Omega \tag{15c}$$

$$\mathbf{f}_{i}^{b\alpha} = \int_{\partial\Omega_e} N_i F_\alpha \overline{t} d\Gamma + \int_{\Omega_e} N_i F_\alpha \mathbf{b} d\Omega \quad (\alpha = 1, 4) \tag{15d}$$

In (15), $\mathbf{B}_i^u$, $\mathbf{B}_i^a$ and $\mathbf{B}_i^b$ are the matrices of shape function derivatives, which are defined as

$$\mathbf{B}_i = \begin{bmatrix} N_{i,x} & 0 \\ 0 & N_{i,y} \\ N_{i,y} & N_{i,x} \end{bmatrix} \tag{16a}$$

$$\mathbf{B}_i^a = \begin{bmatrix} (N_i H)_{,x} & 0 \\ 0 & (N_i H)_{,y} \\ (N_i H)_{,y} & (N_i H)_{,x} \end{bmatrix} \tag{16b}$$

$$\mathbf{B}_i^{b\alpha} = \begin{bmatrix} (N_i F_\alpha)_{,x} & 0 \\ 0 & (N_i F_\alpha)_{,y} \\ (N_i F_\alpha)_{,y} & (N_i F_\alpha)_{,x} \end{bmatrix} \quad (\alpha = 1, 4) \tag{16c}$$

4 Enrichment functions

Crack-tip enrichment functions are defined by the set of functions that span the asymptotic fields around the crack-tip [6]. Such displacement fields are given in (9) for a plane anisotropic solid. By expanding the summation in (9), these asymptotic displacements may be expressed as follows:

$$\begin{aligned} u_1(r,\theta) =& \sqrt{\frac{2r}{\pi}} [K_I (\Re\{A_{11} B_{11}^{-1} \beta_1 + A_{12} B_{21}^{-1} \beta_2\}) \\ &+ K_{II} (\Re\{A_{11} B_{12}^{-1} \beta_1 + A_{22} B_{22}^{-1} \beta_2\})] \end{aligned} \tag{17a}$$

$$\begin{aligned} u_2(r,\theta) =& \sqrt{\frac{2r}{\pi}} [K_I (\Re\{A_{21} B_{11}^{-1} \beta_1 + A_{22} B_{21}^{-1} \beta_2\}) \\ &+ K_{II} (\Re\{A_{21} B_{12}^{-1} \beta_1 + A_{22} B_{22}^{-1} \beta_2\})] \end{aligned} \tag{17b}$$

where

$$\beta_i = \sqrt{\cos\theta + \mu_i \sin\theta} \tag{17c}$$

and μ_i are the eigenvalues from (8) with the positive imaginary part.

Therefore, four crack-tip enrichment functions may be directly derived from (17a) and (17b), to yield

$$F_l(r,\theta) = \sqrt{r}\begin{pmatrix} \Re\{A_{11}B_{11}^{-1}\beta_1 + A_{12}B_{21}^{-1}\beta_2\} \\ \Re\{A_{11}B_{12}^{-1}\beta_1 + A_{12}B_{22}^{-1}\beta_2\} \\ \Re\{A_{21}B_{11}^{-1}\beta_1 + A_{22}B_{21}^{-1}\beta_2\} \\ \Re\{A_{21}B_{12}^{-1}\beta_1 + A_{22}B_{22}^{-1}\beta_2\} \end{pmatrix} \tag{18}$$

which may be expressed in matrix form as

$$\mathbf{F}(r,\theta) = \sqrt{r}\left(\Re\left[\frac{\mathbf{B}^{-1}\mathbf{A}_1\boldsymbol{\beta}}{\mathbf{B}^{-1}\mathbf{A}_2\boldsymbol{\beta}}\right]\right) \tag{19}$$

where $\mathbf{A}_1$ and $\mathbf{A}_2$ correspond to the first and second row of matrix $\mathbf{A}$, respectively, and

$$\boldsymbol{\beta} = \begin{bmatrix} \beta_1 & 0 \\ 0 & \beta_2 \end{bmatrix} \tag{20}$$

The matrices $\mathbf{A}$ and $\mathbf{B}$ depend only on the material properties, but are independent of the adopted coordinate system and the geometry of the problem. In contrast to the isotropic enrichment functions, the anisotropic enrichment functions depend on the material properties of the domain, and are concisely obtained using the Stroh's formalism. It should be remarked that, from a mathematical point of view, Stroh's formalism is valid for anisotropic material behavior laws and it does not further lead to the isotropic enrichment functions, since this is a degenerate case where repeated roots occur for the characteristic equation of the material. However, the derived enrichment functions for anisotropic materials may be readily applied to the isotropic case by simply introducing a small perturbation to one of the repeated Stroh's eigenvalues, leading to stable and precise results as well.

5 Computation of the stress intensity factors

As in previous extended finite element studies [2, 13], we adopt the domain form of the contour interaction integral to calculate the stress intensity factors (SIFs). In order to make this paper self-contained, a brief description of this approach follows.

The classical path independent J-integral is expressed by [18]

$$J = \int_{\Gamma_q} (W\delta_{1j} - \sigma_{ij}u_{i,1})n_j \, d\Gamma_q \tag{21}$$

where the indexes i and j vary from 1 to 2 in a two-dimensional solid, Γ_q is an arbitrary closed contour that contains the crack-tip, n_j is the j-th component of the outward unit vector normal to such a contour, and W is the strain energy density, which for a linear material can be expressed as

$$W = \frac{1}{2}(\sigma_{ij}\varepsilon_{ij}) \tag{22}$$

Applying the divergence theorem to (21) the following equivalent domain expression may be obtained for homogeneous materials:

$$J = \int_A (\sigma_{ij}u_{i,1} - W\delta_{1j})q_{,j} \, dA \tag{23}$$

where A is the area inside the contour Γ_q and q is an arbitrary smoothing function such that it is unity at the crack tip and zero on Γ_q.

Next, let us consider two independent states: a principal one, which is the object of interest and denoted as state (1), and an auxiliary state, denoted as (2). This auxiliary state may be chosen to coincide with the crack-tip asymptotic field, so that it satisfies both equilibrium and the traction-free boundary condition on the crack surface. Such auxiliary state is expressed in terms of the generalized Stroh's formalism [24, 27] in (9) and (10).

The superposition of these two states produces another equilibrium state [2, 13] for which the J-integral is

$$J^{(S)} = \int_A \left((\sigma_{ij}^{(1)} + \sigma_{ij}^{(2)})(u_{i,1}^{(1)} + u_{i,1}^{(2)}) - W^{(S)}\delta_{1j}\right) q_{,j} dA \tag{24}$$

with

$$W^{(S)} = \frac{1}{2}\left[(\sigma_{ij}^{(1)} + \sigma_{ij}^{(2)})(\varepsilon_{ij}^{(1)} + \varepsilon_{ij}^{(2)})\right] \tag{25}$$

The J-integral in (24) can be further decomposed into three distinct integrals as

$$J^{(S)} = J^{(1)} + J^{(2)} + M^{(1,2)} \tag{26}$$

where $M^{(1,2)}$ is the interaction integral, defined as

$$M^{(1,2)} = \int_A (\sigma_{ij}^{(1)}u_{i,1}^{(2)} + \sigma_{ij}^{(2)}u_{i,1}^{(1)} - W^{(1,2)}\delta_{1j})q_{,j} dA \tag{27}$$

with

$$W^{(1,2)} = \frac{1}{2}(\sigma_{ij}^{(1)}\varepsilon_{ij}^{(2)} + \sigma_{ij}^{(2)}\varepsilon_{ij}^{(1)}) \tag{28}$$

The J-integral is related to the energy release rate, and it may be written in terms of the SIFs as [26]:

$$J = \frac{1}{2}\mathbf{K}_N\mathbf{Y}\mathbf{K}_N^T \tag{29}$$

where $\mathbf{K}_N = [K_I \quad K_{II}]$ and $\mathbf{Y}$ is the (2×2) Irwin matrix, which depends on the material properties

$$\mathbf{Y} = \Re(i \cdot \mathbf{A}\mathbf{B}^{-1})$$

where $\mathbf{A}$ and $\mathbf{B}$ are defined in (8).

Thus, for plane problems, the following relation holds for every equilibrium state

$$J = \frac{1}{2}K_{II}^2 Y_{11} + \frac{1}{2}K_I^2 Y_{22} + K_I K_{II} Y_{12} \tag{30}$$

Substituting this expression into (26), the interaction integral $M^{(1,2)}$ can be rewritten as

$$\begin{aligned} M^{(1,2)} =& K_{II}^{(1)} K_{II}^{(2)} Y_{11} + K_I^{(1)} K_I^{(2)} Y_{22} + \\ & (K_I^{(1)} K_{II}^{(2)} + K_{II}^{(1)} K_I^{(2)}) Y_{12} \end{aligned} \tag{31}$$

The individual mode I and mode II SIFs may be evaluated by solving the system of linear algebraic equations obtained from (31) by choosing appropriate auxiliary states. If the auxiliary state is chosen so that $K_I^{(2)} = 1$ and $K_{II}^{(2)} = 0$, (31) is reduced to

$$M^{(1,I)} = K_I^{(1)} Y_{22} + K_{II}^{(1)} Y_{12} \tag{32}$$

whereas selecting an auxiliary state satisfying $K_I^{(2)} = 0$ and $K_{II}^{(2)} = 1$, (31) is reduced to

$$M^{(1,II)} = K_{II}^{(1)} Y_{11} + K_I^{(1)} Y_{12} \tag{33}$$

Therefore, the determination of the SIF is reduced to solve the following system of linear equations:

$$\begin{pmatrix} M^{(1,II)} \\ M^{(1,I)} \end{pmatrix} = \mathbf{Y} \begin{pmatrix} K_{II}^{(1)} \\ K_I^{(1)} \end{pmatrix} \tag{34}$$

6 Numerical results

The performance of the proposed enrichment functions is evaluated by solving several fracture problems. A convergence study is further conducted to characterize our approach. To this end, the obtained results are compared with available solutions in the literature, derived either analytically or numerically by means of the boundary element method (BEM) [11, 23].

In all simulations bi-linear quadrilateral elements are used, with a 2×2 Gaussian quadrature for non-enriched finite elements and a 5×5 quadrature for elements with enriched nodes but not cut by the crack. The elements cut by the crack are partitioned into triangles [8], as Figure 4 illustrates, and a 7 point triangular Gaussian quadrature is used within each subtriangle.

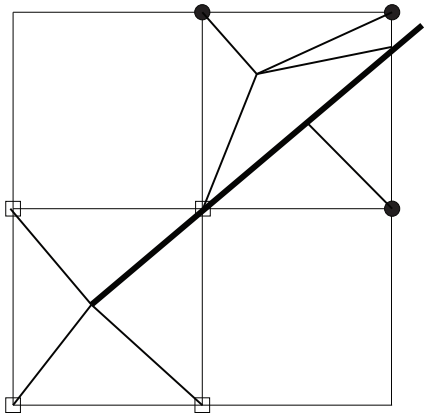

Fig. 4 Partitioning elements that are cut by a crack.

6.1 Convergence study

Consider an anisotropic plate occupying $[0, 2a]^2$, with a center-crack of length a with crack-tips located at $(a/2, a)$ and $(3a/2, a)$. The material properties of the anisotropic plate are given by: $C_{11} = 90.6448$ GPa, $C_{12} = 23.7448$ GPa, $C_{16} = 41.2055$ GPa, $C_{22} = 23.8568$ GPa, $C_{26} = 16.6346$ GPa and $C_{66} = 30.9390$ GPa.

The Dirichlet conditions corresponding to $K_I = 1$ and $K_{II} = 0$ are imposed on the boundaries. Convergence is analyzed in terms of the relative error in the energy norm, defined as

$$E_{rel} = \frac{||\mathbf{u} - \mathbf{u}^*||_{E(\Omega)}}{||\mathbf{u}^*||_{E(\Omega)}} = \frac{(\int_\Omega (\boldsymbol{\varepsilon} - \boldsymbol{\varepsilon}^*)^T \mathbf{C} (\boldsymbol{\varepsilon} - \boldsymbol{\varepsilon}^*) d\Omega)^{1/2}}{(\int_\Omega \boldsymbol{\varepsilon}^{*T} \mathbf{C} \boldsymbol{\varepsilon}^* d\Omega)^{1/2}}$$

where the superscript $*$ refers to the exact analytical solution for the displacement and strain fields.

Figure 5 shows the obtained relative error in the energy norm versus the mesh density on a logarithmic scale. Results are obtained for both topological and geometrical enrichment strategies. The geometrical fixed area enrichment is done for two radii of the enriched domain, namely $r_e/a = 0.2$ and $r_e/a = 0.3$. Furthermore, two sets of enrichment functions are considered: the newly derived anisotropic crack-tip functions proposed in this work, and the simpler enrichment functions for isotropic solids [9], namely

$$F_{iso}(r, \theta) = \left\{ \sqrt{r}\cos\frac{\theta}{2}, \sqrt{r}\sin\frac{\theta}{2}, \sqrt{r}\sin\frac{\theta}{2}\sin\theta, \sqrt{r}\cos\frac{\theta}{2}\sin\theta \right\}$$

It can be noticed that the errors in the energy norm calculated with topological enrichment are similar when using either the anisotropic or the isotropic crack-tip functions. However, differences are apparent with geometrical enrichment. For this case, although isotropic enrichment leads to a reasonable approximation with a simpler enrichment function, the error in the energy norm obtained with the isotropic enrichment functions

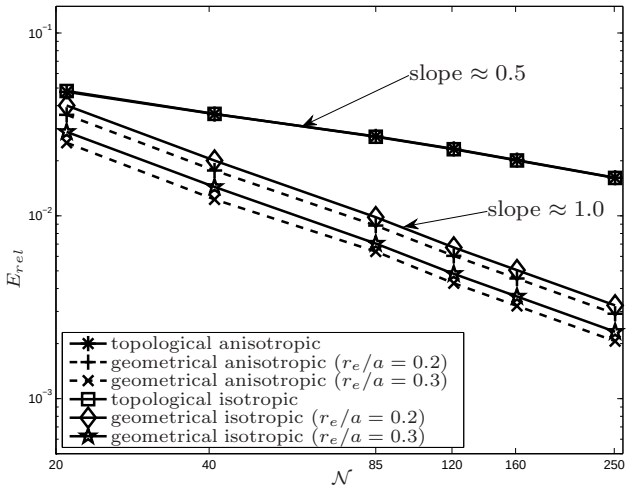

Fig. 5 Relative energy norm for different types of crack-tip enrichments.

is about 10% larger than the one obtained with the anisotropic enrichment functions. Convergence rates are in accordance with finite element theory and consistent with previous extended finite element studies [14, 25]: slopes of approximately 0.5 and 1 are obtained when using topological and geometrical enrichment, respectively.

6.2 Center-crack in an orthotropic plate

A square plate ($h/w = 1$) with a center-crack of length $2a$ under uniform traction at two opposite sides is analyzed (Figure 6). The size of the crack is defined by $a/w = 0.2$. Results are obtained using topological and geometrical enrichment (fixed area with $r_e/a = 0.3$), as well as with both the enrichment functions derived in this work for anisotropic behavior and the simpler isotropic enrichment functions.

Different material properties are considered. The shear modulus and the Poisson's ratio are fixed: $G_{12} = 6$ GPa and $\nu_{12} = 0.03$, and the Young moduli E_1 and E_2 are calculated from the expressions:

$$E_1 = G_{12}(\varphi + 2\nu_{12} + 1) \tag{35}$$

$$E_2 = E_1/\varphi \tag{36}$$

with φ being a material parameter defined by the ratio between Youngs moduli. The numerical results are compared with those obtained using the boundary element method in References [11, 23] and the extended finite element method in Reference [2].

The plate is discretized using two different $N_e \times N_e$ meshes, with $N_e = 45$ and $N_e = 85$. The normalized mode I SIF ($K_I/(\sigma\sqrt{\pi a})$), calculated for several values

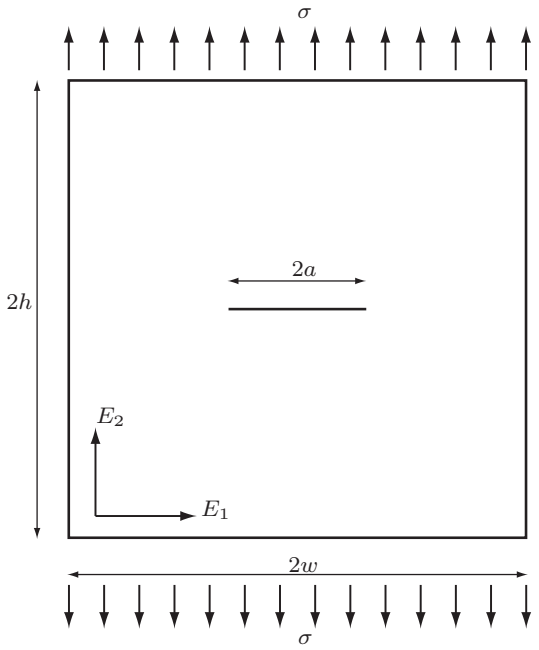

Fig. 6 Square plate with a center-crack under uniform traction.

of the material parameter φ are shown in Figures 7 and 8 for the $N_e = 45$ and the $N_e = 85$ meshes, respectively.

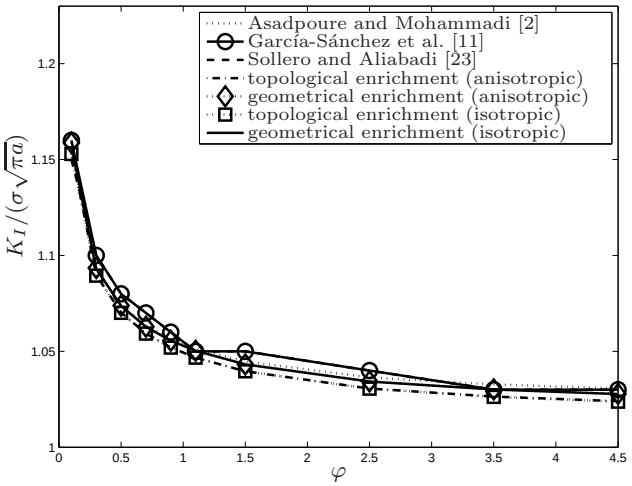

Fig. 7 Results for the orthotropic square plate with a center-crack (45×45 FE mesh).

It can be observed that the results obtained with X-FEM are in good agreement with the ones calculated via BEM and with the orthotropic X-FEM enrichment functions. Moreover, the geometrical enrichment leads to a slightly better approximation as compared to the topological enrichment. The difference in between the adopted reference BEM results [11] and the X-FEM results is shown in Table 1 for the two FE meshes, as

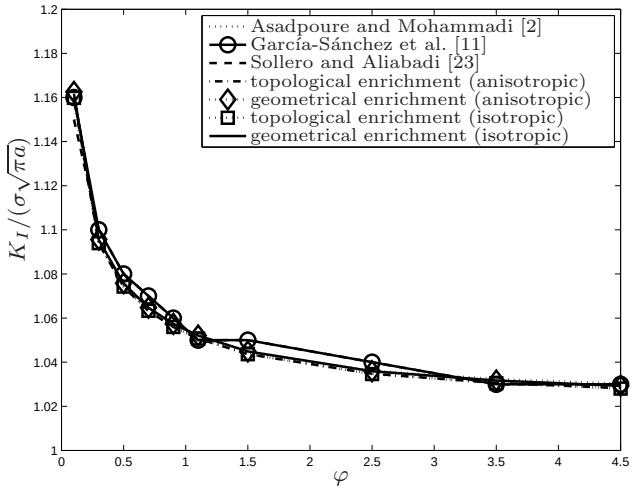

Fig. 8 Results for the orthotropic square plate with a center-crack (85 × 85 FE mesh).

well as for the different enrichment strategies and crack-tip enrichment functions considered. Results are shown with a precision of four decimal digits so that comparisons to those obtained using isotropic enrichment functions can be made.

Table 1 Difference (%) between the normalized mode I SIF obtained with X-FEM and the reference BEM solution [11]. Orthotropic plate with center-crack.

φ	45 × 45 mesh			
	Anisotropic		Isotropic	
	Topological	Geometrical	Topological	Geometrical
0.1	0.4399	0.1097	0.4926	0.2413
0.3	0.8684	0.5986	0.8699	0.6294
0.5	0.8329	0.5740	0.8307	0.5849
0.7	0.9211	0.6685	0.9193	0.6722
0.9	0.6677	0.4191	0.6670	0.4198
1.1	0.2173	0.0286	0.2181	0.0290
1.5	0.8856	0.6468	0.8893	0.6466
2.5	0.7795	0.5476	0.7907	0.5508
3.5	0.2141	0.0167	0.2321	0.0097
4.5	0.4413	0.2116	0.4654	0.2220
φ	85 × 85 mesh			
	Anisotropic		Isotropic	
	Topological	Geometrical	Topological	Geometrical
0.1	0.0323	0.2187	0.0609	0.1469
0.3	0.5883	0.3968	0.5881	0.4140
0.5	0.5726	0.3915	0.5706	0.3977
0.7	0.6693	0.4937	0.6679	0.4958
0.9	0.4207	0.2483	0.4202	0.2487
1.1	0.0263	0.1968	0.0259	0.1971
1.5	0.6504	0.4851	0.6527	0.4847
2.5	0.5546	0.3945	0.5607	0.3957
3.5	0.0069	0.1656	0.0023	0.1622
4.5	0.2231	0.0659	0.2349	0.0713

6.3 Double edge-crack in an anisotropic plate

A square plate ($h/w = 1$) with a double edge-crack ($a/w = 0.5$) is considered. The plate is subjected to a uniform traction applied on opposite sides, as depicted in Figure 9.

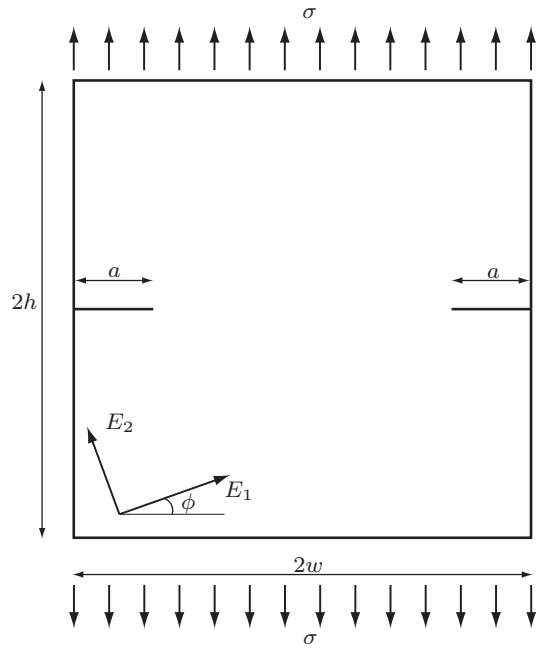

Fig. 9 Square plate with double edge-crack under uniform traction.

The plate is a symmetric angle ply composite laminate consisting of four graphite-epoxy laminae, with the following elastic properties: $E_1 = 144.8$ GPa, $E_2 = 11.7$ GPa, $G_{12} = 9.66$ GPa and $\nu_{12} = 0.21$. To analyze the influence of the fiber orientation on the SIF, the fibers are rotated from $\phi = 0°$ to $\phi = 90°$.

Due to the symmetry of the problem, only half of the plate is discretized, using two different meshes with 45×95 and 85×175 elements, respectively. Figures 10 and 11 present the variation of the mode I normalized SIF $K_I/(\sigma\sqrt{\pi a})$ with respect to the direction of the fibers ϕ for each mesh. The normalized SIF calculated with X-FEM show good agreement with the reference BEM solutions [11, 23]. As expected, better results are obtained when using the finer mesh with geometrical enrichment (with $r_e/a = 0.3$).

The difference between the X-FEM results and the reference BEM solution [11] are given in Table 2 for the 85×175 mesh.

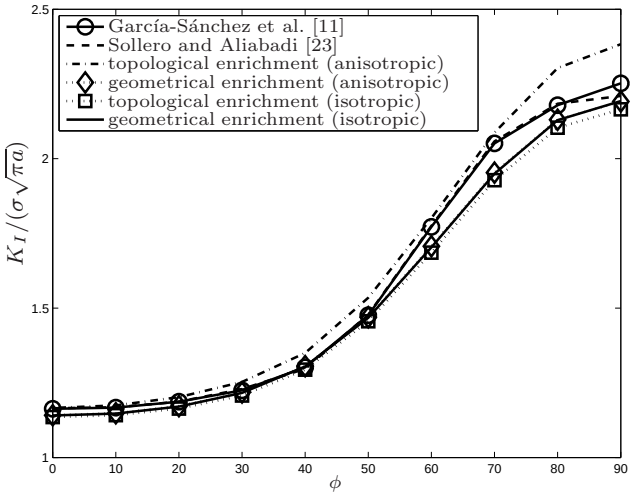

Fig. 10 Results for the anisotropic square plate with a double edge-crack (45×95 FE mesh).

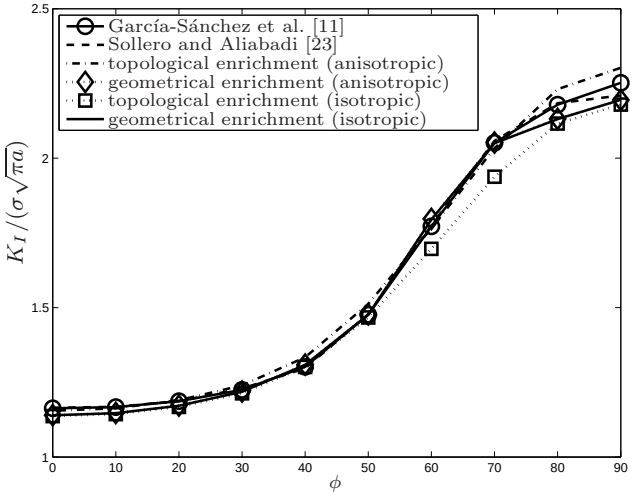

Fig. 11 Results for the anisotropic square plate with a double edge-crack (85×175 FE mesh).

Table 2 Difference (%) between the normalized mode I SIF obtained with X-FEM and the reference BEM solution [11]. Plate with double edge-crack.

$\phi(^\circ)$	Anisotropic		Isotropic	
	Topological	Geometrical	Topological	Geometrical
0°	2.3827	2.1387	2.4300	2.1759
10°	2.0287	1.7646	2.0765	1.8033
20°	1.5723	1.2415	1.6303	1.2894
30°	1.2332	0.7937	1.2994	0.8480
40°	0.3971	0.9580	0.3501	0.9058
50°	0.7346	0.0557	0.7591	0.1322
60°	4.4156	2.4605	4.4188	2.5704
70°	5.8270	3.8994	5.8253	3.9919
80°	3.1199	2.4017	3.1228	2.4335
90°	1.3978	0.6911	1.3907	0.6614

6.4 Slanted center-crack in an anisotropic plate

A rectangular plate ($h/w = 2$) with an inclined center-crack is considered (see Figure 12). Uniform traction is applied on opposite sides of the plate. The material is a glass-epoxy composite with properties: $E_1 = 48.26$ GPa, $E_2 = 17.24$ GPa, $G_{12} = 6.89$ GPa and $\nu_{12} = 0.29$. The crack length is $2a = 0.4w$ and the crack is inclined at an angle of 45°. The directions of the fibers are rotated from $\phi = 0^\circ$ to 180°.

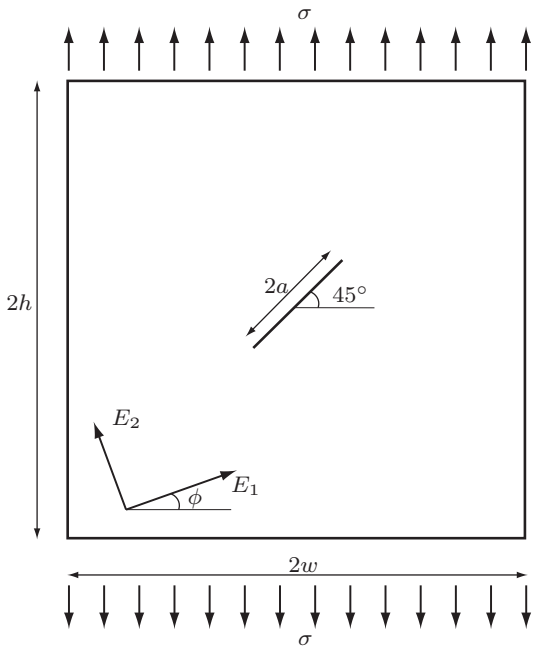

Fig. 12 Slanted center-crack under uniform traction.

The numerical results are given in Figure 13 for the normalized mode I SIF ($K_I/\sigma\sqrt{\pi a}$) and in Figure 14 for the normalized mode II SIF ($K_{II}/\sigma\sqrt{\pi a}$), considering a 85×175 mesh. As in previous examples, a normalized radius of $r_e/a = 0.3$ was adopted for the geometrical enrichment.

Good agreement is observed between the obtained X-FEM results and the reference BEM solution [11]. Differences between both sets of results are given in Tables 3 and 4.

Table 3 Difference (%) between the normalized mode I SIF obtained with X-FEM and the reference BEM solution [11]. Plate with slanted center-crack.

ϕ	Anisotropic		Isotropic	
	Topological	Geometrical	Topological	Geometrical
0°	0.1516	0.0962	0.1717	0.0819
45°	1.1000	0.5624	1.0582	0.5048
90°	1.1449	0.9689	1.9120	1.7344
105°	1.8646	1.7598	2.6425	2.5376
120°	1.9719	1.8644	2.7595	2.6561
135°	1.9912	1.8579	2.7603	2.6226
180°	0.1516	0.0962	0.1717	0.0819

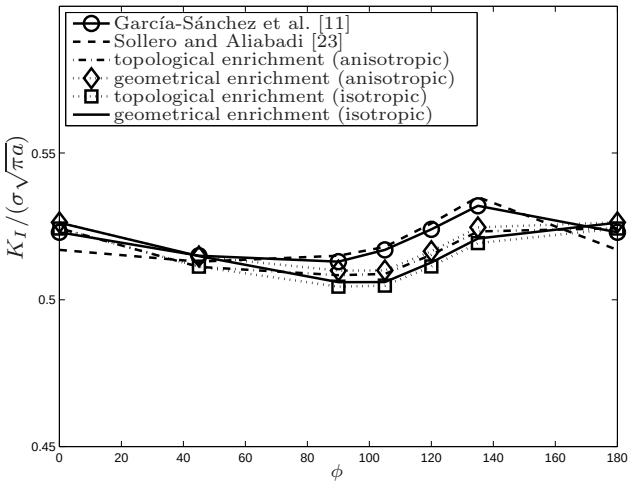

Fig. 13 Normalized mode I SIF for a slanted center-crack (85×175 FE mesh).

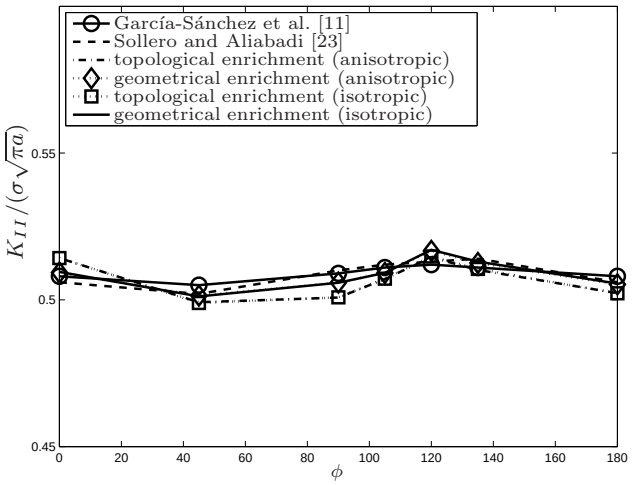

Fig. 14 Normalized mode II SIF for a slanted center-crack (85×175 FE mesh).

7 Concluding remarks

In this paper, we presented an extended finite element formulation for the analysis of fracture problems in plane fully anisotropic materials. New crack-tip enrichment functions were derived in a compact form using Stroh's formalism. Fracture parameters were accurately computed by means of the interaction integral method. Several crack configurations were analyzed, and the accuracy of the obtained results compared favorably with those available in the literature [11, 23]. Results based on anisotropic crack-tip enrichment functions was compared with those obtained using isotropic crack-tip functions. Furthermore, both topological and geometrical enrichment strategies were adopted, and it was demonstrated that the latter yielded better accuracy at the optimal rate of convergence in energy. Although the differences between both types of enrichment are small, the anisotropic enrichment function provide better results than the isotropic ones. The proposed formulation is versatile and can be extended to model coupled phenomena such as thermoelasticity, piezoelectricity and magnetoelectroelasticity. Moreover, the new enrichment functions allow one to explore other types of problems, such as crack identification in fully anisotropic two-dimensional materials.

Table 4 Difference (%) between the normalized mode II SIF obtained with X-FEM and the reference BEM solution [11]. Plate with slanted center-crack.

ϕ	Anisotropic		Isotropic	
	Topological	Geometrical	Topological	Geometrical
0°	0.3451	1.0546	0.3026	1.0808
45°	1.6632	1.4036	1.6648	1.3965
90°	1.8654	0.9698	1.8555	0.9723
105°	0.9673	0.6836	0.9614	0.6816
120°	0.2618	0.5503	0.2842	0.5850
135°	0.4615	0.1919	0.4340	0.1528
180°	2.0109	1.8399	2.0534	1.8661

Acknowledgements This work was funded by the *Ministerio de Ciencia e Innovación*, Spain, research project DPI2010-21590-C02-02.

References

1. Abbas, S., Fries, T.P.: A unified enrichment scheme for fracture problems. IOP Conference Series: Materials Science and Engineering **10**(1), 012,045 (2010)
2. Asadpoure, A., Mohammadi, S.: Developing new enrichment functions for crack simulation in orthotropic media by the extended finite element method. International Journal for Numerical Methods in Engineering **69**, 2150–2172 (2007)
3. Babuška, I., Melenk, J.M.: The partition of unity method. International Journal for Numerical Methods in Engineering **4**, 607–632 (1997)
4. Béchet, E., Minnebo, H., Möes, N., Burgardt, B.: Improved implementation and robustness study of the x-fem for stress analysis around cracks. International Journal for Numerical Methods in Engineering **64**, 1033–1056 (2005)
5. Béchet, E., Scherzer, M., Kuna, M.: Application of the X-FEM to the fracture of piezoelectric materials. International Journal for Numerical Methods in Engineering **77**, 1535–1565 (2009)
6. Belytschko, T., Black, T.: Elastic crack growth in finite elements with minimal remeshing. International Journal for Numerical Methods in Engineering **45**, 601–620 (1999)
7. Boone, T.J., Wawrzynek, P.A., Ingraffea, A.R.: Finite element modelling of fracture propagation in orthotropic materials. Engineering Fracture Mechanics **26**, 185–201 (1987)
8. Dolbow, J., Moës, N., Belytschko, T.: An extended finite element method for modeling crack growth with frictional

contact. Computer Methods in Applied Mechanics and Engineering **190**, 6825–6846 (2001)
9. Fleming, M., Chu, Y.A., Moran, B., Belytschko, T.: Enriched element-free Galerkin methods for crack tip fields. International Journal for Numerical Methods in Engineering **40**, 1483–1504 (1997)
10. Fries, T.P., Belytschko, T.: The extended/generalized finite element method: An overview of the method and its applications. International Journal for Numerical Methods in Engineering **84**, 253–304 (2010)
11. García-Sánchez, F., Sáez, A., Domínguez, J.: Traction boundary elements for cracks in anisotropic solids. Engineering Analysis with Boundary Elements **28**, 667–676 (2004)
12. Laborde, P., Pommier, J., Renard, Y., Salaün, M.: High-order extended finite element method for cracked domains. International Journal for Numerical Methods in Engineering **64**, 354–381 (2005)
13. Moës, N., Dolbow, J., Belytschko, T.: A finite element method for crack growth without remeshing. International Journal for Numerical Methods in Engineering **46**, 131–150 (1999)
14. Mousavi, S.E., Sukumar, N.: Generalized gaussian quadrature rules for discontinuities and crack singularities in the extended finite element method. Computer Methods in Applied Mechanics and Engineering **199**(49-52), 3237–3249 (2010)
15. Muskhelishvili, N.I.: Some basic problems of the mathematical theory of elasticity, 2nd edn. Leiden: Noordhoff (1953)
16. Nobile, L., Carloni, C.: Fracture analysis for orthotropic cracked plates. Composite Structures **68**(3), 285–293 (2005)
17. Pan, E., Amadei, B.: Fracture mechanics analysis of cracked 2-d anisotropic media with a new formulation of the boundary element method. International Journal of Fracture **77**, 161–74 (1996)
18. Rice, J.R.: A path independent integral and the approximate analysis of strain concentration by notches and cracks. Journal of Applied Mechanics **35**, 379–386 (1968)
19. Rojas-Díaz, R., Sukumar, N., Sáez, A., García-Sánchez, F.: Fracture in magnetoelectroelastic materials using the extended finite element method. International Journal for Numerical Methods in Engineering (2011). DOI: 10.1002/nme.3219
20. Sih, G.C., Paris, P.C., Irwin, G.R.: On cracks in rectilinearly anisotropic bodies. International Journal of Fracture **1**, 189–203 (1965)
21. Sladek, J., Sladek, V., Atluri, S.: Meshless local petrov-galerkin method in anisotropic elasticity. Computer Modeling in Engineering and Sciences **6**, 477–489 (2004)
22. Sollero, P., Aliabadi, M.: Fracture mechanics analysis of anisotropic plates by the boundary element method. International Journal of Fracture **64**, 269–284 (1993)
23. Sollero, P., Aliabadi, M.H.: Anisotropic analysis of cracks in composite laminates using the dual boundary element method. Composite Structures **31**, 229–33 (1995)
24. Stroh, A.: Dislocation and cracks in anisotrpic elasticity. Philosophical magazine **3**, 625–646 (1958)
25. Sukumar, N., Huang, Z.Y., Prévost, J.H., Suo, Z.: Partition of unity enrichment for bimaterial interface cracks. International Journal for Numerical Methods in Engineering **59**, 1075–1102 (2004)
26. Suo, Z.: Singularities, interfaces and cracks in dissimilar anisotropic media. Proc. R. Soc. Lond. A **427**, 331–358 (1990)
27. Ting, T.C.T.: Anisotropic Elasticity. Oxford University Press, New York (1996)